THE JOURNAL OF PHYSICAL CHEMISTRY C

Article

pubs.acs.org/JPCC

Unified Theoretical Framework for Realizing Diverse Regimes of Strong Coupling between Plasmons and Electronic Transitions

Jacob A. Faucheaux,[†,∥] Jiayi Fu,[†,⊥,∥] and Prashant K. Jain*[,†,‡,§,∥]

[†]Department of Chemistry, [‡]Materials Research Lab, and [§]Department of Physics, University of Illinois Urbana−Champaign , Urbana, Illinois 61801, United States

Supporting Information

ABSTRACT: Strong coupling between light and quantum mechanical transitions historically observed in atomic optics is now being realized in the solid state using plasmon resonances. Recent experiments on hybrid plasmonic/excitonic systems have reported varied observations such as excitonic splitting, asymmetric line shapes, and dips in scattering spectra. Here, we unite these seemingly disparate empirical observations under a single theoretical framework, illustrating that the same generalized hybrid system allows access to diverse forms of coupling between plasmons and molecular transitions. Simply by modifying the damping rate of the plasmon resonance, it is possible to transition from one regime of coupling to another (e.g., from Rabi splitting to Fano interference). Common experimental handles such as size, shape, and nature of the metal can be varied to tune the regime of coupling, as shown by electrodynamic simulations. We also show that strong coupling can be achieved using simple nanostructure configurations such as a plasmonic core/excitonic shell geometry without the necessity of sophisticated design of near-field hotspots. The unified model developed here will allow rational predictive design of hybrid plasmonic systems for achieving unique control of light on the nanoscale.

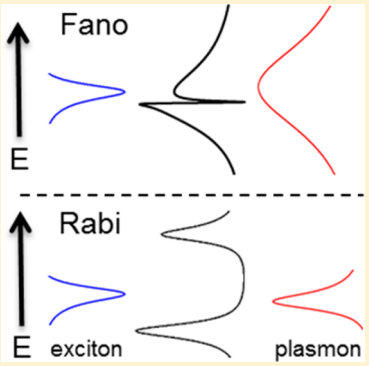

INTRODUCTION

Research in atomic optics has allowed exquisite control of quantum mechanical transitions by electromagnetic radiation. The ability to manipulate electronic transitions using light has always been of fundamental interest, but these phenomena also show promise in optical computing,[1−3] light harvesting,[4] and ultrasensitive detection.[5−7] Strong coupling between atomic transitions and electromagnetic radiation is typically achieved by excitation of atoms with precisely tuned laser beams[8,9] or by placement of atoms in high-quality resonant cavities.[10,11]

However, such phenomena are now being realized in the solid state using hybrids of plasmonic and excitonic materials, also termed plexcitonic systems.[12] In these systems, strongly confined light in the form of a localized surface plasmon resonance[13−25] (LSPR) serves the role of a laser field or a resonant cavity mode.[26−28] Several recent experimental studies on plexcitonic systems have reported various phenomena: energy shifts in excitonic spectra,[29] absorption dips in plasmon resonance spectra,[30−32] Rabi splitting,[33−35] and Fano line shapes.[36−42] Each one of these observations is indeed a manifestation of coupling between plasmons and excitons; however, there is no physical understanding of why such a diverse range of phenomena is observed, or why a specific phenomenon is observed in a specific experiment. While some theoretical work has been done, it has mainly focused on fitting individual empirical observations.[43−48]

Here, we provide a simple classical electrodynamic framework that unites seemingly disparate phenomena observed thus far in plexcitonic systems. We show using an analytic model and electrodynamic simulations that (i) Each one of the observed phenomena is simply a subset of a generalized form of coupling between a plasmonic oscillator and an excitonic resonance. In other words, there exist various regimes of coupling between the plasmon resonance and the excitonic resonance. (ii) It is possible to tune the system from one type of coupling to another simply by variation of the damping rate of the plasmonic oscillator. For instance, narrow-line width plasmon resonances induce Rabi splitting of the excitonic transition, whereas heavily damped plasmon resonances exhibit Fano interference with the excitonic transition. (iii) Tuning between coupling regimes can be achieved by use of common experimental handles like nanoparticle size, shape, and nature of the metal. (iv) Simple configurations, e.g., a plasmonic core/molecular shell geometry, can be used to achieve various forms of strong coupling. Sophisticated design of near-field hotspots does not seem necessary. The plasmon damping rate is the most important parameter that dictates coupling.

This generalized model highlights the remarkable degree of control over light−matter coupling possible with plasmon resonant systems. The model will enable experimentalists to make physical assignments of observed phenomena, while identifying potential artifacts. A priori prediction of the nature of coupling will also be possible. While early efforts in the field have been empirical, the model developed here will facilitate

Received: December 12, 2013
Revised: January 7, 2014
Published: January 9, 2014

   dx.doi.org/10.1021/jp412157c | J. Phys. Chem. C 2014, 118, 2710−2717

rational design of hybrid nanostructures for plasmonic manipulation of excitonic systems and realization of exotic forms of light−matter interactions in the solid state.

METHODS

In order to support the conclusions of the analytic model developed here, scattering spectra of hybrid plasmonic/excitonic nanostructures were simulated. The discrete dipole approximation (DDA) method was used for these simulations.[49,50] DDA numerically solves Maxwell's equations by discretizing the target geometry into an array of virtual point dipoles and self-consistently solving for the polarizability of each virtual dipole. We employed the DDSCAT 7.3.0 code from Draine and Flatau. Excitation of the target nanostructure was achieved by a linearly polarized plane wave.

The hybrid nanostructure was simulated by a plasmonic nanoparticle coated with a patchy shell of molecular excitonic absorbers. Virtual point-dipole arrays representing a plasmonic core/excitonic shell nanostructure were generated using the DDSCAT subroutine calltarget. In order to render the molecular shell patchy, representative of actual samples in experiments, a random number generator was used to remove 1/4 of the virtual point dipoles comprising the shell. Furthermore, the molecular shell was made discontinuous by removing a strip of dipoles around the center of the nanostructure normal to the incident light polarization direction. This procedure is necessary to prevent the splitting of the molecular shell resonance into an inner- and an outer-shell resonance, which is a nonphysical effect for a molecular shell where electrons are not completely delocalized.

For the study of nanoparticle size dependence, the radius of the nanoparticle core (r_{core}) was varied from 5.5 to 100.5 nm, while the volume fraction of the core $(r_{core}/r_{shell})^3$ was kept fixed at 0.715 by appropriate variation of the shell thickness. For shape dependence, spheroidal core/shell nanoparticles of varying aspect ratio were investigated. The total volume of the core/shell nanostructure was kept constant at ca. 6367 nm^3. The light polarization direction was maintained along the long axis. Simulations for nanospheres of r_{core} = 37.5 nm and r_{core} = 50.5 nm were performed with an interdipole spacing of 2 nm. Simulations for nanospheres of r_{core} = 100.5 nm nanospheres were performed with an interdipole spacing of 4 nm, and all other simulations utilized a dipole spacing of 1 nm.

A medium dielectric constant of 1.00 was used for all calculations. The dielectric function of the molecular excitonic shells was modeled by a Lorentzian oscillator.

$$\varepsilon(\omega) = \varepsilon_\infty - f\frac{\omega_0^2}{\omega^2 - \omega_0^2 + i\omega\gamma} \tag{1}$$

where ε_∞ = 2.5 is the high-frequency dielectric constant typical of a dye aggregate[33] and f = 0.1 is the oscillator strength. ω_0 is the frequency of the exciton chosen to be resonant with the LSPR frequency, and γ is the exciton line width with a value of 0.05 eV, as used in past work.[33] We do not consider nonlocal effects resulting from the delocalized nature of the exciton.[51] The excitons in dye aggregates are only delocalized over a few molecules; the resulting nonlocality may cause additional effects but does not seem necessary to reproduce key phenomena[33,43] observed in plexcitonic systems.

Bulk experimental dielectric functions from Johnson and Christy[52] were employed for the plasmonic nanoparticle core. For a study of the effect of the metal, spherical nanoparticles (r_{core} = 10.5 nm) of different metals Au, Ag, and Cu were investigated. In order to investigate the role of interband damping, the Au dielectric function (ε_{exp}) was modified by removing the imaginary part of the interband contribution (ε_{IB}) as described by Sheikholeslami et al.:[53]

$$\mathrm{Im}(\varepsilon_{IB}) = \mathrm{Im}(\varepsilon_{exp}) - \frac{\gamma_p\omega_p^2}{\omega(\omega^2 + \gamma_p^2)} \tag{2}$$

where Im implies imaginary part, ω_p is the bulk plasma frequency of Au with a value of 9.1 eV, and γ_p is the bulk electron collision frequency with a value of 0.073 eV for Au.

RESULTS AND DISCUSSION

Analytical Model. Coupling in the plexcitonic system can be described by the classical electrodynamic interaction of two Lorentzian oscillators,[54] one representing the excitonic resonance and the other representing the plasmon resonance with a tunable damping rate. The excitonic and plasmonic polarizabilities in the dipolar quasistatic limit are given as

$$\alpha_{ex} = \frac{1}{A}; \quad \alpha_p = \frac{F}{A - iB} \tag{3}$$

where $A = \omega_0^2 - \omega^2$, ω_o is the resonance frequency of both oscillators. Note we consider only the resonant case, which is a necessary condition for achieving strong coupling effects of interest in plexcitonic systems. $B = \omega\Gamma$ is a tunable parameter, where Γ is the plasmon line width (eV), which signifies the damping rate of the plasmon. F is the magnitude of the oscillator strength of the plasmon resonance in units of nm^3 eV^2 normalized to a value of 1 nm^3 eV^2 for the oscillator strength of the excitonic resonance. The oscillator strength is directly proportional to the number of electrons (N) in the system, which is equal to the electron density (n) times the nanoparticle volume (V). Since the bulk plasma frequency ω_p^2 is proportional to n, F is proportional to the product of the bulk plasma frequency and the volume, thus having units of nm^3 eV^2. The polarizability has units of nm^3. For calculations based on our analytic model, we use a value of F = 500, which is physically reasonable: for instance, a 10-nm radius silver nanosphere has ca. 250 000 free electrons, 500 times more than the number of electronic oscillators in a surface coating consisting of 500 dye molecules. We assume the line width of the excitonic resonance is much smaller than the frequencies considered, so it is neglected. In the dipolar quasistatic limit used here, multipolar and retardation effects are not included, allowing the analytical expressions to take easy-to-visualize forms. The DDA simulations presented later take into account these finite size effects, allowing us to verify that these effects, while potentially necessary for quantitative modeling of experimental spectra, do not alter the general nature of phenomena predicted by the analytic model of plexcitonic coupling.

While the electrodynamic coupling between the plasmonic oscillator and excitonic oscillator is a multipolar interaction in the strictest sense, we consider only the most important dipole−dipole interaction in our analytic model, an approach that has been successful at qualitative modeling of plasmon/plasmon and plasmon/exciton coupling.[21,43,44,53,55] DDA simulations presented later consider the full multipolar interaction. In the dipole−dipole coupling approximation, the polarizability of the coupled plasmonic/excitonic system is given as[53,55]

dx.doi.org/10.1021/jp412157c | J. Phys. Chem. C 2014, 118, 2710−2717

$$\alpha' = \frac{\alpha_{ex}(1 + \kappa\alpha_p) + \alpha_p(1 + \kappa\alpha_{ex})}{1 - \kappa^2\alpha_{ex}\alpha_p} \quad (4)$$

where $\kappa = 2(1/(4\pi \cdot d^3))$ is the coupling constant with units of nm^{-3}. The factor 2 is the orientation factor corresponding to a head-to-tail arrangement of the two dipoles,[53,55] and d is the distance between the center of mass of the two dipoles. Since eq 4 has κ^2 in its denominator, the expression contains solutions for both in-phase (parallel) and out-of-phase (antiparallel) coupling of the two oscillators, as shown below in eq 8.

The scattering cross section of the plexcitonic system is obtained from the polarizability as

$$C_{sca} = \frac{k^4}{6\pi}|\alpha'|^2 \quad (5)$$

where k is the wave-vector. From eqs 3 and 4, we get

$$|\alpha'|^2 = \frac{B^2}{A^2B^2 + (A^2 - \kappa^2F)^2} + \frac{(A(1 + F) + 2F\kappa)^2}{A^2B^2 + (A^2 - \kappa^2F)^2} \quad (6)$$

We consider two extreme regimes of coupling:

Regime 1, where the plasmon resonance has an extremely narrow line width. In other words, the damping rate of the plasmonic oscillator is extremely small when compared to optical frequencies ($\Gamma \ll \omega$). In this regime, B can be neglected, thus yielding

$$|\alpha'|^2 = \frac{((\omega_0^2 - \omega^2)(1 + F) + 2F\kappa)^2}{((\omega_0^2 - \omega^2)^2 - \kappa^2F)^2} \quad (7)$$

The poles of this expression predict two resonant modes at frequencies given by

$$\omega = \sqrt{\omega_0^2 \pm \kappa\sqrt{F}} \quad (8)$$

This case represents plasmon resonance-induced Rabi splitting of the excitonic mode into lower and higher energy hybridized modes, as illustrated in Scheme 1. The splitting energy is determined by the relative oscillator strengths (F) and the coupling constant (κ).

The plasmonic oscillator, in the narrow-line width regime, serves as a solid-state analogue of a cavity mode of extremely high finesse, needed for achieving Rabi splitting.

Regime 2, where the plasmon line width is extremely large. In other words, the damping rate of the plasmon is much larger than the frequencies considered ($\Gamma \gg \omega$). In this case, $B \gg A^2$ and the expression for the coupled polarizability given by

$$|\alpha'|^2 = \frac{1}{A^2 + \left(\frac{A^2}{B} - \frac{\kappa^2F}{B}\right)^2} + \left(\frac{1 + F}{B}\right)^2 \frac{\left(A + \left(\frac{2F}{1 + F}\right)\kappa\right)^2}{A^2 + \left(\frac{A^2}{B} - \frac{\kappa^2F}{B}\right)^2} \quad (9)$$

reduces to

Scheme 1. Illustration of Rabi Splitting in a Hybrid Plasmonic/Excitonic System[a]

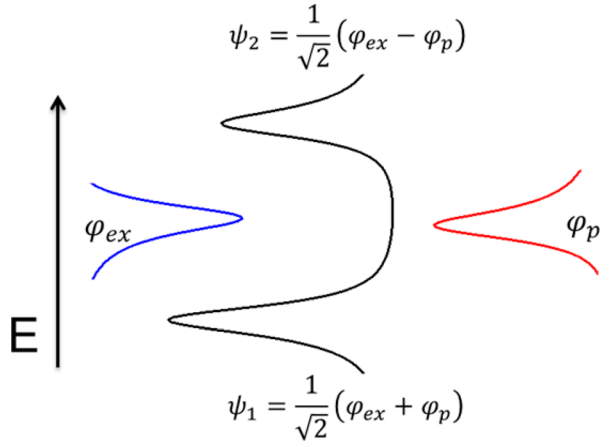

[a]A plasmonic oscillator with a sufficiently narrow line width couples strongly with an excitonic resonance to produce two hybridized modes split in energy.

$$|\alpha'|^2 = \frac{1}{(\omega_0^2 - \omega^2)^2 + \left(\frac{\kappa^2F}{B}\right)^2} + \left(\frac{1 + F}{B}\right)^2 \frac{\left(\omega_0^2 - \omega^2 + \left(\frac{2F}{1 + F}\right)\kappa\right)^2}{(\omega_0^2 - \omega^2)^2 + \left(\frac{\kappa^2F}{B}\right)^2}$$

(Lorentzian peak) + (Fano interference term) (10)

The spectrum effectively represents a Fano line shape (second term) superimposed on the excitonic Lorentzian oscillator (first term) with a peak frequency of ω_0 and a peak broadening of κ^2F/B. Thus, in the regime where the plasmonic oscillator is extremely damped, the plasmon resonance behaves like a broad-band continuum. This continuum undergoes interference with the excitonic resonance to give rise to a Fano line shape (Scheme 2).

Thus, eq 7 (Rabi splitting) and eq 10 (Fano interference) represent two extreme regimes of a generalized model of

Scheme 2. Illustration of Fano Line Shape in a Hybrid Plasmonic/Excitonic System[a]

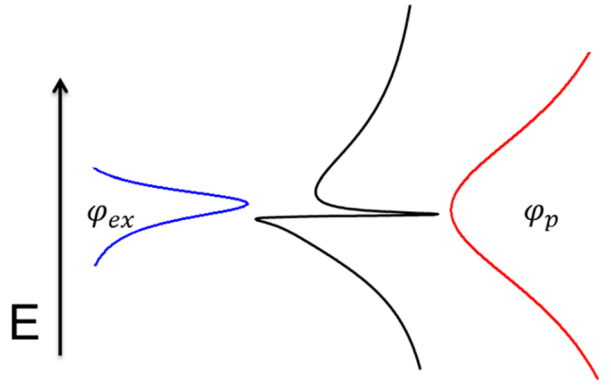

[a]A plasmonic oscillator with an extremely broad line width resembles a continuum of states and undergoes Fano interference with the excitonic resonance.

dx.doi.org/10.1021/jp412157c | J. Phys. Chem. C 2014, 118, 2710−2717

coupling between the plasmonic oscillator and the excitonic resonance (eq 6). The line width or damping rate of the plasmonic oscillator is the physical parameter that dictates the nature of coupling. Scattering spectra calculated from the unified expression (eq 6) indeed illustrate a gradual transition from Rabi splitting to Fano interference as the damping rate of the plasmonic oscillator is increased from Γ = 0.01 eV to Γ = 0.50 eV (Figure 1A). Furthermore, the predicted Rabi splitting energies are on the order of 100 meV, which is consistent with previous reports.[31,33−35,44]

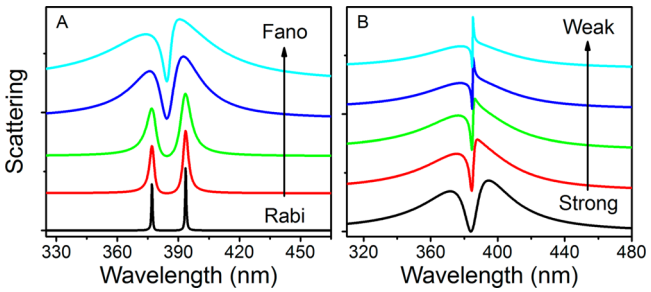

Figure 1. Generalized model of plasmonic/excitonic coupling predicting various distinct regimes of coupling. (A) A coupled oscillator model shows that as the damping rate or line width (Γ) of the plasmonic resonator is increased, there is a transition from a Rabi splitting regime (Γ = 0.01 eV) to a Fano interference regime (Γ = 0.50 eV). Intermediate cases (Γ = 0.05, 0.1, and 0.3 eV) are also shown to demonstrate the gradual evolution between the two regimes. F = 500 and κ = 0.020 nm^{-3}, for all calculations. The range of Γ values employed here is physically reasonable; for instance, homogeneous line widths of silver nanospheres are in the 0.05−0.5 eV range depending on the nanoparticle size and the medium refractive index.[57] (B) Decreasing the value of the coupling constant κ results in a transition from an antiresonance feature in the Lorentzian spectrum (κ = 0.027 nm^{-3}) to an asymmetric line shape superimposed on the Lorentzian spectrum (κ = 0.0059 nm^{-3}). Intermediate cases (κ = 0.0150, 0.0115, and 0.0073 nm^{-3}) demonstrate the gradual transition between these two Fano regimes. F = 500 and Γ = 0.5 eV, for all calculations. The range of values of κ (0.027−0.0057 nm^{-3}) is equivalent to a dipole−dipole separation distance ranging from 1.8 to 3.0 nm, which is physically reasonable.

Further insight into the nature of coupling is gained by direct comparison of the Fano interference term in eq 10 to Ugo Fano's expression:[56]

$$C_{sca} = \frac{\left(E - E_{res} + q\frac{L}{2}\right)^2}{(E - E_{res})^2 + \left(\frac{L}{2}\right)^2} \tag{11}$$

Here E is the energy, E_{res} is the resonant energy, L is the resonance line width, and q is the Fano parameter, which is a ratio of the resonant scattering to the background scattering amplitude. When q approaches zero, the Fano expression takes the form of an antiresonance (a dip in absorption at E_{res}). When q is greater than zero, the expression takes the form of the familiar Fano asymmetric line shape. By analogy to the Fano expression, we determine the q parameter for the plasmonic/excitonic system from eq 10:

$$q = \frac{B}{\kappa}\left(\frac{2}{1+F}\right) \tag{12}$$

Thus, we find that the plexcitonic Fano parameter is inversely proportional to the relative oscillator strength F of the plasmon and the coupling constant κ. In the limit of very strong coupling (large values of κ and/or F), $q \to 0$, and eq 10 predicts a dip in the Lorentzian spectrum at the frequency ω_0:

$$|\alpha'|^2 = \frac{1}{(\omega_0^2 - \omega^2)^2 + \left(\frac{\kappa^2 F}{B}\right)^2} + \left(\frac{1+F}{B}\right)^2 \left(1 - \frac{\left(\frac{\kappa^2 F}{B}\right)^2}{(\omega_0^2 - \omega^2)^2 + \left(\frac{\kappa^2 F}{B}\right)^2}\right)$$

$$\text{(Lorentzian peak)} + \text{(dip at } \omega_0\text{)} \tag{13}$$

This antiresonance feature represents a form of electromagnetically induced transparency (EIT), achieved by a plasmon resonance in lieu of a laser or cavity. For smaller values of κ and/or F, $q > 0$, and eq 10 predicts an asymmetric line shape superimposed on the Lorentzian spectrum. Indeed, scattering spectra calculated from eq 4 demonstrate that as the coupling strength is decreased (by a reduction in κ), the scattering spectrum transitions from an antiresonance feature to the asymmetric Fano line shape (Figure 1B).

Electrodynamic Simulations. Thus, our generalized model successfully predicts three distinct regimes of coupling: Rabi splitting, an antiresonance Fano regime or EIT, and an

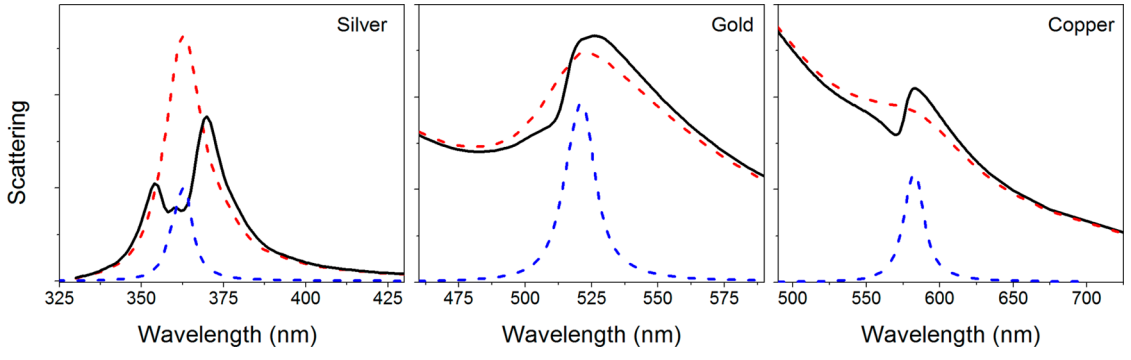

Figure 2. Nature of the metal influences regime of coupling. A change from a low-loss metal (silver) to a high-loss metal (gold or copper) leads to a transition from Rabi splitting of the molecular resonance to Fano interference between plasmon and exciton. The spectra shown are DDA-calculated scattering spectra for metal nanoparticle core/excitonic shell nanostructures with r_{core} = 10.5 nm and 1-nm thick (patchy) shells. Purely plasmonic scattering spectra with nonresonant shells (calculated using f = 0) are shown for reference by the dashed red curve. The excitonic resonance is also shown for reference by the dashed blue curve.

dx.doi.org/10.1021/jp412157c | J. Phys. Chem. C 2014, 118, 2710−2717

asymmetric Fano regime. The coupling regime can be controlled through the plasmonic damping rate. We set out to perform electrodynamic simulations to identify common experimental handles for achieving such control. As a model system, we employed a configuration consisting of a plasmonic nanoparticle core coated with a patchy shell of molecules with an excitonic resonance. Such a system is easy to realize experimentally: dye aggregates with a well-defined excitonic resonance are known to form on metal nanoparticle surfaces.[58,59] Some promising observations have already been made in such nanostructures.[41,60−62]

Using our DDA simulations, we first considered the effect of the nature of the plasmonic metal. Silver, gold, and copper are three widely studied plasmonic metals due to their LSPRs, which span the visible spectrum. Discrete dipole approximation (DDA) calculated scattering spectra for r_{core} = 10.5 nm nanospheres with a 1-nm thick excitonic shell are shown in Figure 2. Small silver nanospheres (r_{core} < 20 nm) are characterized by narrow line widths[63] (small B in eq 6), due to low intrinsic damping in silver. Consistently, silver nanoparticle core/excitonic shell nanostructures demonstrate two well-separated peaks in the calculated scattering spectrum. These separated peaks are indicative of the Rabi splitting regime, where the LSPR line width is sufficiently narrow. On the contrary, LSPRs of small gold and copper nanospheres suffer from heavy damping due to the effect of overlapping interband transitions and are therefore significantly broadened (large B in eq 6). The calculated scattering spectra of gold and copper nanoparticle core/excitonic shell nanostructures are reminiscent of the weak-coupling Fano regime. Both gold and copper demonstrate an asymmetric line shape superimposed over the original scattering spectrum.

We next consider the effect of nanoparticle size on coupling. It is known that small silver nanoparticles exhibit low damping, whereas radiative damping in silver nanoparticles increases dramatically with size. Increased radiative damping at larger sizes leads to significantly broadened and red-shifted silver scattering spectra as illustrated in Figure 3. This broadening has a drastic effect on the observed coupling regime. Whereas small silver nanospheres (r_{core} = 25.5 nm or lesser) exhibit splitting into well-resolved scattering peaks as expected for Rabi splitting, larger nanospheres (r_{core} = 37.5 nm or greater) lie in the antiresonance Fano regime. As the size increases from r_{core} = 37.5 nm to r_{core} = 100.5 nm, the magnitude of the antiresonance dip decreases. Interestingly, even the r_{core} = 100.5 nm silver core/excitonic shell nanostructure, despite its extremely high radiative damping, does not transition into the asymmetric Fano line shape regime that is seen in gold and copper nanospheres. Even though radiative decay is able to damp the plasmonic oscillator, it does not sufficiently reduce the coupling to allow a transition to the asymmetric Fano regime.

To elucidate the effect of nanoparticle shape on coupling, we choose ellipsoidal gold nanostructures, motivated by the ease of synthesis of gold nanorods.[64] The gold nanorod LSPR is highly dependent on the aspect ratio (AR) of the nanorod.[23,65] Figure 4 shows DDA-calculated scattering spectra of ellipsoidal gold nanoparticle core/excitonic shell nanostructures of varying aspect ratio but fixed volume. The AR = 1 nanostructure is clearly in the asymmetric Fano regime. As the AR is increased, there is a red shift of the LSPR accompanied by a narrowing of the LSPR line width, due to the decreased overlap between the LSPR and interband transitions of gold.[65] This decrease in the

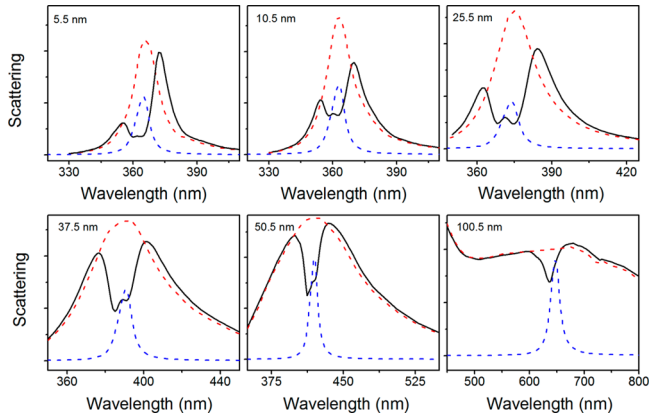

Figure 3. Nanoparticle size is a handle for tuning of the coupling regime. An increase in size (from r_{core} = 5.5 nm to r_{core} = 100.5 nm) results in a progression from a Rabi splitting regime to a Fano interference regime. Increase in nanoparticle size is responsible for increasing the radiative damping of the plasmonic oscillator. The spectra shown are DDA-calculated scattering spectra for silver nanoparticle core/excitonic shell nanostructures with a constant volume fraction of ca. 0.715. Purely plasmonic scattering spectra with nonresonant shells (calculated using f = 0) are shown for reference by the dashed red curve. The excitonic resonance is also shown for reference by the dashed blue curve.

LSPR line width leads to a gradual diminution of the asymmetry and a transition from the Fano coupling regime (AR = 1) to the Rabi splitting regime (AR = 4).

We finally consider the direct role of interband damping on the type of coupling. We performed this study by removing the imaginary part of the interband contribution to the dielectric function of gold, as described in Methods. While this is not physically realizable, it is instructive for understanding how electronic properties of the metal influence coupling of the plasmon resonance with excitons. Figure 5 shows DDA-calculated scattering spectra of r_{core} = 10.5 nm gold nanospheres coated with 1-nm thick excitonic shells. The gold nanosphere with the unmodified dielectric function shows the Fano line shape, as shown earlier. However, removal of the interband contribution results in a transition to the Rabi splitting regime. This clearly illustrates how severely interband damping affects excitonic coupling. Interband transitions of gold heavily damp the LSPR, resulting in the observation of the Fano regime. In addition, interband damping in gold also causes significantly reduced coupling strength. This is evidenced by the asymmetric line shapes observed with gold nanospheres, which are not seen with large silver nanospheres, despite the significant radiative damping of the latter. As demonstrated in Figure 4, nanoparticle shape offers a handle for decoupling plasmon resonances from interband transitions by reducing the spectral overlap between the two, allowing better control over the coupling regime.

Previous experimental scattering spectra of single gold nanospheres coated with resonant dye aggregates agree extremely well with our calculated scattering spectrum for the spherical gold core/excitonic shell system.[60] Original attempts to model this experimental data with the analytic core/shell Mie expression greatly exaggerated the observed effect due to the unrealistic nature of the continuous shell. Our randomly generated patchy shells more accurately describe the optical behavior of a polycrystalline dye aggregate coated on the surface of a metal nanoparticle. It is important to note that the

dx.doi.org/10.1021/jp412157c | J. Phys. Chem. C 2014, 118, 2710−2717

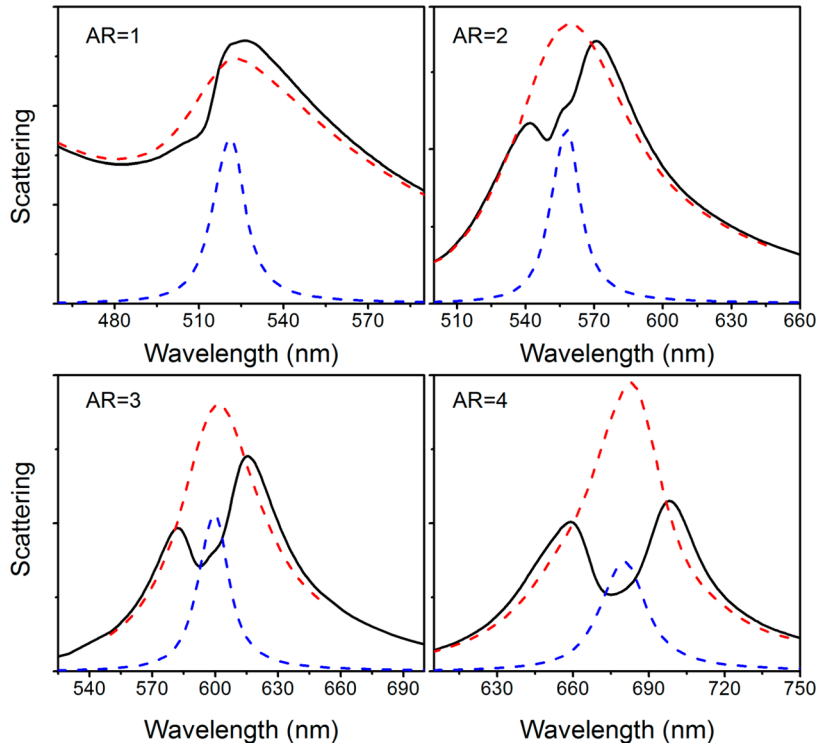

Figure 4. Coupling regime can be tuned via a variation in nanoparticle shape. As the aspect ratio (AR) increases from 1 to 4, there is a transition from Fano interference to Rabi splitting. The increasing aspect ratio leads to a decrease of the LSPR line width and consequently a decrease in Fano type character. The spectra shown are DDA-calculated scattering spectra for ellipsoidal gold nanoparticle core/excitonic shell nanostructures with a constant volume of ca. 6367 nm^3. Purely plasmonic scattering spectra with nonresonant shells (calculated using $f = 0$) are shown for reference by the dashed red curve. The excitonic resonance is also shown for reference by the dashed blue curve.

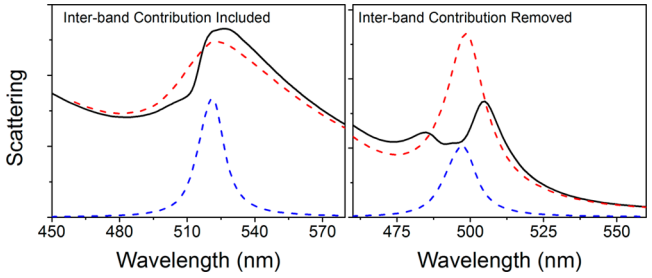

Figure 5. Interband damping influences the coupling regime achievable. DDA-calculated scattering spectra show that by artificially removing overlapping interband transitions, the plasmon line width decreases resulting in a transition from Fano interference (pure gold dielectric function) to a Rabi splitting regime (gold dielectric function with imaginary part of the interband contribution removed). Purely plasmonic scattering spectra with nonresonant shells (calculated using $f = 0$) are shown for reference by the dashed red curve. The excitonic resonance is also shown for reference by the dashed blue curve.

coupling effect observed with gold nanospheres (i.e., Fano line shape superimposed on the plasmonic scattering spectrum) is perceptibly small and could easily be missed without precise measurements. Silver nanospheres and gold nanorods have not been experimentally explored as yet, but our simulations show that these nanostructures can offer much more dramatic spectral effects, due to the absence of interband damping of the LSPR.

Many experimental studies have utilized junctions of plasmonic nanoparticles as platforms for achieving strong coupling motivated by the high electromagnetic field enhancements in these junctions.[33,35,44] While this approach has been successful, we demonstrate that simple geometries (such as plasmonic core/excitonic shell configurations) are sufficient to access diverse forms of coupling. It is also realized that intense electromagnetic field hotspots are not the principal requirement for achieving strong coupling effects like Rabi splitting. Rather, low damping (narrow line width or high quality factor) and large oscillator strength of the LPSR mode are the physical parameters crucial for observing large energy splitting. Intense electromagnetic fields, while often confused to be the cause, are simply an effect of the large polarizability and high spectral quality of nanostructures that exhibit strong coupling.[66]

■ CONCLUSION

In conclusion, we have provided a unified theoretical framework for understanding and predicting the nature of coupling in hybrid plasmonic/excitonic systems. First, the model illustrates that various regimes of coupling are possible, which are essentially subsets of a generalized form of coupling between a plasmon and an exciton. Second, the model demonstrates that transitions between different regimes can be accomplished. The damping rate or line width of the plasmon resonance is the most critical physical parameter that governs the regime of coupling. Narrow-line width plasmon resonances are necessary for Rabi splitting of the excitonic resonance, whereas heavily damped plasmon resonances exhibit Fano interference with the excitonic resonance. We also showed using simulations that the damping rate and consequently the regime of coupling can be controlled through common experimental handles such as nanoparticle size, shape, and metal. In particular, we identified small silver nanospheres and gold nanorods of high aspect ratio as promising candidates

dx.doi.org/10.1021/jp412157c | J. Phys. Chem. C 2014, 118, 2710−2717

for achieving Rabi splitting, while gold and copper nanospheres, which suffer from heavy interband damping, display only asymmetric Fano line shapes. It is hoped that these findings will encourage experimentalists to explore nanostructures that have thus far not been tested but are predicted to be very promising. The demonstration that simple configurations are sufficient for achieving strong coupling can be especially motivating. The model developed here is expected to guide experimentalists in assigning their observations to a specific type of plasmon/exciton coupling or in choosing relevant parameters when designing a hybrid plasmonic/excitonic system optimized for a specific form of light−matter interaction (e.g., optical transparency). This work is a step toward theory-driven design of hybrid plasmonic systems.

■ ASSOCIATED CONTENT

Supporting Information

Derivation of the dipolar coupling model. This material is available free of charge via the Internet at http://pubs.acs.org.

■ AUTHOR INFORMATION

Corresponding Author

*E-mail: jain@illinois.edu.

Present Address

[⊥]School of Engineering, Cooper Union, New York, NY 10003.

Author Contributions

[∥]J.A.F performed simulations, data analysis, and cowrote the manuscript. J.F. performed preliminary simulations. P.K.J. developed analytic theory, performed data analysis, and cowrote the manuscript.

Notes

The authors declare no competing financial interest.

■ ACKNOWLEDGMENTS

This material is based upon work supported by the National Science Foundation Graduate Research Fellowship Program under grant no. DGE-1144245 (J.A.F) and the Dupont Young Professor Award (P.K.J.). J.F. carried out work as part of a REU program funded by the National Science Foundation and 3M. This work used the Extreme Science and Engineering Discovery Environment (XSEDE) which is supported by National Science Foundation grant no. OCI-1053575.

■ REFERENCES

(1) Zhang, J. Z.; Noguez, C. Plasmonic Optical Properties and Applications of Metal Nanostructures. *Plasmonics* **2008**, *3*, 127−150.

(2) Khitrova, G.; Gibbs, H. M.; Kira, M.; Koch, S. W.; Scherer, A. Vacuum Rabi Splitting in Semiconductors. *Nat. Phys.* **2006**, *2*, 81−90.

(3) Luk'yanchuk, B.; Zheludev, N. I.; Maier, S. A.; Halas, N. J.; Nordlander, P.; Giessen, H.; Chong, C. T. The Fano Resonance in Plasmonic Nanostructures and Metamaterials. *Nat. Mater.* **2010**, *9*, 707−715.

(4) Hirakawa, T.; Kamat, P. V Charge Separation and Catalytic Activity of Ag@TiO2 Core−Shell Composite Clusters Under UV-Irradiation. *J. Am. Chem. Soc.* **2005**, *127*, 3928−3934.

(5) Liu, N.; Langguth, L.; Weiss, T.; Kästel, J.; Fleischhauer, M.; Pfau, T.; Giessen, H. Plasmonic Analogue of Electromagnetically Induced Transparency at the Drude Damping Limit. *Nat. Mater.* **2009**, *8*, 758−762.

(6) Im, H.; Bantz, K. C.; Lee, S. H.; Johnson, T. W.; Haynes, C. L.; Oh, S.-H. Self-Assembled Plasmonic Nanoring Cavity Arrays for SERS and LSPR Biosensing. *Adv. Mater.* **2013**, *25*, 2678−85.

(7) Mayer, K. M.; Hafner, J. H. Localized Surface Plasmon Resonance Sensors. *Chem. Rev.* **2011**, *111*, 3828−57.

(8) Boller, K.-J.; Imamoglu, A.; Harris, S. E. Observation of Electromagnetically Induced Transparency. *Phys. Rev. Lett.* **1991**, *66*, 2593−2596.

(9) Harris, S. E.; Field, J. E.; Imamoglu, A. Nonlinear Optical Processes Using Electromagnetically Induced Transparency. *Phys. Rev. Lett.* **1990**, *64*, 1107−1110.

(10) Sanchez-Mondragon, J. J.; Narozhny, N. B.; Eberly, J. H. Theory of Spontaneous-Emission Line Shape in an Ideal Cavity. *Phys. Rev. Lett.* **1983**, *51*, 550−553.

(11) Zhu, Y.; Gauthier, D. J.; Morin, S. E.; Wu, Q.; Carmichale, H. J.; Mossberg, T. W. Vacuum Rabi Splitting as a Feature of Linear-Dispersion Theory: Analysis and Experimental Observations. *Phys. Rev. Lett.* **1990**, *64*, 2499−2502.

(12) Manjavacas, A.; García de Abajo, F. J.; Nordlander, P. Quantum Plexcitonics: Strongly Interacting Plasmons and Excitons. *Nano Lett.* **2011**, *11*, 2318−23.

(13) Schatz, G. C. Theoretical Studies of Surface Enhanced Raman Scattering. *Acc. Chem. Res.* **1984**, *17*, 370−376.

(14) Kelly, K. L.; Coronado, E.; Zhao, L. L.; Schatz, G. C. The Optical Properties of Metal Nanoparticles: The Influence of Size, Shape, and Dielectric Environment. *J. Phys. Chem. B* **2003**, *107*, 668−677.

(15) Link, S.; Wang, Z. L.; El-Sayed, M. A. Alloy Formation of Gold−Silver Nanoparticles and the Dependence of the Plasmon Absorption on Their Composition. *J. Phys. Chem. B* **1999**, *103*, 3529−3533.

(16) Connor, E. E.; Mwamuka, J.; Gole, A.; Murphy, C. J.; Wyatt, M. D. Gold Nanoparticles Are Taken Up by Human Cells but Do Not Cause Acute Cytotoxicity. *Small* **2005**, *1*, 325−327.

(17) Millstone, J. E.; Park, S.; Shuford, K. L.; Qin, L.; Schatz, G. C.; Mirkin, C. A. Observation of a Quadrupole Plasmon Mode for a Colloidal Solution of Gold Nanoprisms. *J. Am. Chem. Soc.* **2005**, *127*, 5312−5313.

(18) Shafer-Peltier, K. E.; Haynes, C. L.; Glucksberg, M. R.; Van Duyne, R. P. Toward a Glucose Biosensor Based on Surface-Enhanced Raman Scattering. *J. Am. Chem. Soc.* **2003**, *125*, 588−593.

(19) Storhoff, J. J.; Elghanian, R.; Mucic, R. C.; Mirkin, C. A.; Letsinger, R. L. One-Pot Colorimetric Differentiation of Polynucleotides with Single Base Imperfections Using Gold Nanoparticle Probes. *J. Am. Chem. Soc.* **1998**, *120*, 1959−1964.

(20) Nehl, C. L.; Grady, N. K.; Goodrich, G. P.; Tam, F.; Halas, N. J.; Hafner, J. H. Scattering Spectra of Single Gold Nanoshells. *Nano Lett.* **2004**, *4*, 2355−2359.

(21) Jain, P. K.; Eustis, S.; El-Sayed, M. A. Plasmon Coupling in Nanorod Assemblies: Optical Absorption, Discrete Dipole Approximation Simulation, and Exciton-Coupling Model. *J. Phys. Chem. B* **2006**, *110*, 18243−18253.

(22) Sosa, I. O.; Noguez, C.; Barrera, R. G. Optical Properties of Metal Nanoparticles with Arbitrary Shapes. *J. Phys. Chem. B* **2003**, *107*, 6269−6275.

(23) Jain, P. K.; Lee, K. S.; El-Sayed, I. H.; El-Sayed, M. A. Calculated Absorption and Scattering Properties of Gold Nanoparticles of Different Size, Shape, and Composition: Applications in Biological Imaging and Biomedicine. *J. Phys. Chem. B* **2006**, *110*, 7238−7248.

(24) Slaughter, L.; Chang, W.-S.; Link, S. Characterizing Plasmons in Nanoparticles and Their Assemblies with Single Particle Spectroscopy. *J. Phys. Chem. Lett.* **2011**, *2*, 2015−2023.

(25) Chen, T.; Pourmand, M.; Feizpour, A.; Cushman, B.; Reinhard, B. M. Tailoring Plasmon Coupling in Self-Assembled One-Dimensional Au Nanoparticle Chains through Simultaneous Control of Size and Gap Separation. *J. Phys. Chem. Lett.* **2013**, *4*, 2147−2152.

(26) Galloway, C. M.; Kreuzer, M. P.; Aćimović, S. S.; Volpe, G.; Correia, M.; Petersen, S. B.; Neves-Petersen, M. T.; Quidant, R. Plasmon-Assisted Delivery of Single Nano-Objects in an Optical Hot Spot. *Nano Lett.* **2013**, *13*, 4299−304.

(27) Passmore, B. S.; Adams, D. C.; Ribaudo, T.; Wasserman, D.; Lyon, S.; Davids, P.; Chow, W. W.; Shaner, E. A. Observation of Rabi Splitting from Surface Plasmon Coupled Conduction State Transitions in Electrically Excited InAs Quantum Dots. *Nano Lett.* **2011**, *11*, 338−342.

(28) Ridolfo, A.; Di Stefano, O.; Fina, N.; Saija, R.; Savasta, S. Quantum Plasmonics with Quantum Dot-Metal Nanoparticle Molecules: Influence of the Fano Effect on Photon Statistics. *Phys. Rev. Lett.* **2010**, *105*, 263601.
(29) Zhao, J.; Jensen, L.; Sung, J.; Zou, S.; Schatz, G. C.; Van Duyne, R. P. Interaction of Plasmon and Molecular Resonances for Rhodamine 6G Adsorbed on Silver Nanoparticles. *J. Am. Chem. Soc.* **2007**, *129*, 7647−56.
(30) Choi, Y.; Kang, T.; Lee, L. P. Plasmon Resonance Energy Transfer (PRET)-Based Molecular Imaging of Cytochrome c in Living Cells 2009. *Nano Lett.* **2009**, *9*, 85−90.
(31) Chen, H.; Shao, L.; Woo, K. C.; Wang, J.; Lin, H.-Q. Plasmonic−Molecular Resonance Coupling: Plasmonic Splitting Versus Energy Transfer. *J. Phys. Chem. C* **2012**, *116*, 14088−14095.
(32) Panahpour, A.; Silani, Y.; Farrokhian, M.; Lavrinenko, A. V.; Latifi, H. Coupled Plasmon-Exciton Induced Transparency and Slow Light in Plexcitonic Metamaterials. *J. Opt. Soc. Am. B* **2012**, *29*, 2297.
(33) Schlather, A. E.; Large, N.; Urban, A. S.; Nordlander, P.; Halas, N. J. Near-Field Mediated Plexcitonic Coupling and Giant Rabi Splitting in Individual Metallic Dimers. *Nano Lett.* **2013**, *13*, 3281−3286.
(34) Gómez, D. E.; Vernon, K. C.; Mulvaney, P.; Davis, T. J. Surface Plasmon Mediated Strong Exciton−Photon Coupling in Semiconductor Nanocrystals. *Nano Lett.* **2010**, *10*, 274−278.
(35) Savasta, S.; Saija, R.; Ridolfo, A.; Di Stefano, O.; Denti, P.; Borghese, F. Nanopolaritons: Vacuum Rabi Splitting with a Single Quantum Dot in the Center of a Dimer Nanoantenna. *ACS Nano* **2010**, *4*, 6369−76.
(36) Wu, D.; Jiang, S.; Liu, X. Tunable Fano Resonances in Three-Layered Bimetallic Au and Ag Nanoshell. *J. Phys. Chem. C* **2011**, *115*, 23797−23801.
(37) Svedendahl, M.; Käll, M. Fano Interference between Localized Plasmons and Interface Reflections. *ACS Nano* **2012**, *6*, 7533−7539.
(38) Rahmani, M.; Luk'yanchuk, B.; Hong, M. Fano Resonance in Novel Plasmonic Nanostructures. *Laser Photon. Rev.* **2013**, *7*, 329−349.
(39) Zhang, W.; Govorov, A.; Bryant, G. Semiconductor-Metal Nanoparticle Molecules: Hybrid Excitons and the Nonlinear Fano Effect. *Phys. Rev. Lett.* **2006**, *97*, 146804.
(40) Fan, J. A.; Bao, K.; Wu, C.; Bao, J.; Bardhan, R.; Halas, N. J.; Manoharan, V. N.; Shvets, G.; Nordlander, P.; Capasso, F. Fano-Like Interference in Self-Assembled Plasmonic Quadrumer Clusters. *Nano Lett.* **2010**, *10*, 4680−4685.
(41) Fofang, N. T.; Grady, N. K.; Fan, Z.; Govorov, A. O.; Halas, N. J. Plexciton Dynamics: Exciton−Plasmon Coupling in a J-Aggregate−Au Nanoshell Complex Provides a Mechanism for Nonlinearity. *Nano Lett.* **2011**, *11*, 1556−1560.
(42) Fofang, N. T.; Park, T.-H.; Neumann, O.; Mirin, N. A.; Nordlander, P.; Halas, N. J. Plexcitonic Nanoparticles: Plasmon−Exciton Coupling in Nanoshell−J-Aggregate Complexes. *Nano Lett.* **2008**, *8*, 3481−3487.
(43) Lovera, A.; Gallinet, B.; Nordlander, P.; Martin, O. J. F. Mechanisms of Fano Resonances in Coupled Plasmonic Systems. *ACS Nano* **2013**, *7*, 4527−4536.
(44) Wu, X.; Gray, S. K.; Pelton, M. Quantum-Dot-Induced Transparency in a Nanoscale Plasmonic Resonator. *Opt. Express* **2010**, *18*, 23633−23645.
(45) Chen, X.-W.; Sandoghdar, V.; Agio, M. Coherent Interaction of Light with a Metallic Structure Coupled to a Single Quantum Emitter: From Superabsorption to Cloaking. *Phys. Rev. Lett.* **2013**, *110*, 153605.
(46) Artuso, R. D.; Bryant, G. W. Optical Response of Strongly Coupled Quantum Dot−Metal Nanoparticle Systems: Double Peaked Fano Structure and Bistability. *Nano Lett.* **2008**, *8*, 2106−2111.
(47) Gülen, D. Optical Response of Lorentzian Nanoshells in the Quasistatic Limit. *J. Phys. Chem. B* **2013**, *117*, 11220−11228.
(48) Waks, E.; Sridharan, D. Cavity QED Treatment of Interactions between a Metal Nanoparticle and a Dipole Emitter. *Phys. Rev. A* **2010**, *82*, 043845.
(49) Flatau, P. J.; Draine, B. T. Fast Near Field Calculations in the Discrete Dipole Approximation for Regular Rectinlinear Grids. *Opt. Express* **2012**, *20*, 1247−1252.
(50) Draine, B. T.; Flatau, P. J. Discrete-Dipole Approximation for Scattering Calculations. *J. Opt. Soc. Am. A* **1994**, *11*, 1491.
(51) Teperik, T. V.; Nordlander, P.; Aizpurua, J.; Borisov, A. G. Quantum Effects and Nonlocality in Strongly Coupled Plasmonic Nanowire Dimers. *Opt. Express* **2013**, *21*, 27306.
(52) Johnson, P. B.; Christy, R. W. Optical Constants of the Noble Metals. *Phys. Rev. B* **1972**, *6*, 4370−4379.
(53) Sheikholeslami, S.; Jun, Y.; Jain, P. K.; Alivisatos, A. P. Coupling of Optical Resonances in a Compositionally Asymmetric Plasmonic Nanoparticle Dimer. *Nano Lett.* **2010**, *10*, 2655−60.
(54) Bohren, C.; Huffman, D. *Absorption and Scattering of Light by Small Particles*; John Wiley and Sons: New York, 1998.
(55) Jain, P. K.; Huang, W.; El-Sayed, M. A. On the Universal Scaling Behavior of the Distance Decay of Plasmon Coupling in Metal Nanoparticle Pairs: A Plasmon Ruler Equation. *Nano Lett.* **2007**, *7*, 2080−2088.
(56) Fano, U. Effects of Configuration Interaction on Intensities and Phase Shifts. *Phys. Rev.* **1961**, *124*, 1866−1877.
(57) Hu, M.; Novo, C.; Funston, A.; Wang, H.; Staleva, H.; Zou, S.; Mulvaney, P.; Xia, Y.; Hartland, G. V Dark-Field Microscopy Studies of Single Metal Nanoparticles: Understanding the Factors That Influence the Line Width of the Localized Surface Plasmon Resonance. *J. Mater. Chem.* **2008**, *18*, 1949−1960.
(58) Hranisavljevic, J.; Dimitrijevic, N. M.; Wurtz, G. A.; Wiederrecht, G. P. Photoinduced Charge Separation Reactions of J-Aggregates Coated on Silver Nanoparticles. *J. Am. Chem. Soc.* **2002**, *124*, 4536−7.
(59) Vujačić, A.; Vasić, V.; Dramićanin, M.; Sovilj, S. P.; Bibić, N.; Hranisavljevic, J.; Wiederrecht, G. P. Kinetics of J-Aggregate Formation on the Surface of Au Nanoparticle Colloids. *J. Phys. Chem. C* **2012**, *116*, 4655−4661.
(60) Uwada, T.; Toyota, R.; Masuhara, H.; Asahi, T. Single Particle Spectroscopic Investigation on the Interaction Between Exciton Transition of Cyanine Dye J-Aggregates and Localized Surface Plasmon Polarization of Gold Nanoparticles. *J. Phys. Chem. C* **2007**, *111*, 1549−1552.
(61) Kometani, N.; Tsubonishi, M.; Fujita, T.; Asami, K. Preparation and Optical Absorption Spectra of Dye-Coated Au, Ag, and Au/Ag Colloidal Nanoparticles in Aqueous Solutions and in Alternate Assemblies. *Langmuir* **2001**, 578−580.
(62) Salomon, A.; Wang, S.; Hutchison, J. A.; Genet, C.; Ebbesen, T. W. Strong Light−Molecule Coupling on Plasmonic Arrays of Different Symmetry. *Chemphyschem* **2013**, *14*, 1882−6.
(63) Hodak, H.; Martini, I.; Hartland, G. V Spectroscopy and Dynamics of Nanometer-Sized Noble Metal Particles. *J. Phys. Chem. B* **1998**, *102*, 6958−6967.
(64) Jana, N. R.; Gearheart, L.; Murphy, C. J. Wet Chemical Synthesis of High Aspect Ratio Cylindrical Gold Nanorods. *J. Phys. Chem. B* **2001**, *105*, 4065−4067.
(65) Sönnichsen, C.; Franzl, T.; Wilk, T.; von Plessen, G.; Feldmann, J. Drastic Reduction of Plasmon Damping in Gold Nanorods. *Phys. Rev. Lett.* **2002**, *88*, 077402.
(66) Jain, P. K.; El-Sayed, M. A. Surface Plasmon Resonance Sensitivity of Metal Nanostructures: Physical Basis and Universal Scaling in Metal Nanoshells. *J. Phys. Chem. C* **2007**, *111*, 17451−17454.